# LVRT Control Strategy of DFIG based Wind Turbines Combining Passive and Active Protection

Aboubakr El Makrini*‡, Yassir El Karkri*, Youness Boukhriss*,
Hassane El Markhi*, Hassan El Moussaoui*

* The Signals, Systems and Components Laboratory, Sidi Mohamed Ben Abdellah University, FST Fez, 30000, Morocco

(aboubakr.elmkrini@usmba.ac.ma, yassir.elkarkri@usmba.ac.ma, youness.boukhris@usmba.ac.ma,
hassane.elmarkhi@usmba.ac.ma, hassan.elmoussaoui@usmba.ac.ma)

‡ Corresponding Author: Aboubakr EL MAKRINI; 30000, Tel: +212661105926, aboubakr.elmakrini@usmba.ac.ma

*Received: 02.02.2017 Accepted:12.03.2017*

**Abstract-** Due to its advantages, Doubly Fed Induction Generator (DFIG) is the most used generator in the wind power area. However, the DFIG provides electrical power at a constant frequency even if the rotor speed varies; also, it allows a better capture of wind energy. Although the DFIG has a high sensitivity regarding the electrical faults, which brings up many challenges in terms of compliance: Power provider and electrical operator (in terms of production continuity and quality of energy). Actually, the grid connection requirements impose strict rules to respect for Low Voltage Ride Through (LVRT) and grid support capabilities following the Grid Code (GC). Therefore, it's crucial for wind turbines (WT) to propose an advanced control. In fact, when detecting voltage dips, WTs must stay connected to the grid to provide the required reactive power in order to have a safe and reliable operation. The objective of this article is to propose a new LVRT strategy able to keep WTs connected to the grid despite severe voltage dips. The principle of this strategy is to make a connection between the level of dips and the optimal solution to overcome the fault. For this reason, the proposed strategy is based on the combination of two solutions (an active and a passive method): The first aims to improve the control strategy to mitigate the over-current at low voltage dips. The second is applied for severe voltage dips using protection circuits: Series Dynamic Braking Resistor (SDBR) and DC-Chopper.

**Keywords** Wind power, DFIG, LVRT, Active method, Passive method.

## 1. Introduction

The electricity produced from fossil and nuclear energy has increased significantly over these last years. In fact, those classical sources of energy have a serious environment impact. Therefore, the emerging ecological awareness has greatly increased the interest in renewable energies integration [1]. Wind energy is one of these several clean energies sources. This technology has been having a fast development and has been reached a level of maturity for these last years. So its integration in the grid has a big interest by researchers [2].

In the past, during a grid fault, WT generators (WTGs) has disconnected from the GRID. Actually, to remain these WTs connected to GRID even if a fault occurs, new requirements exist. In fact, during these last years, many countries have established their GCs in transmission and distribution. These codes define voltage conditions ranges for which WTGs have to keep remain connected to the power system [3]. As WTGs become larger and level of penetration becomes higher in the grid, so the grid operators had to modify the GCs [4].

LVRT is a part of the GC established for the grid voltage dips, such as WTGs are required to keep connected to the grid for a considered time before being allowed to disconnect. This considered time can be different from one GC to another depends on the severity of the fault. Fig.1 shows differences among these codes during voltage dips in different countries [5, 6, 7].

Several solutions for LVRT capability have been proposed and classified into two categories. (i) The passive method based on adding some power components to the system. (ii) The active method uses control strategies applied to the DFIG converters. Some passive methods for LVRT had been used. However, the most popular one is to add a

crowbar circuit to isolate the RSC from the rotor windings [8]. To limit over-voltage in the DC-link, a DC-Chopper circuit and parallel capacitors are introduced in [9, 10]. Dynamic braking resistors placed in series with the stator to limit rotor and stator over-currents [11]. For the same reason, a bridge-type fault current limiter is proposed in [12]. Series connected converter [13] and a dynamic voltage restorer [14, 15] are added to the system to keep the stator voltage stable during grid faults.

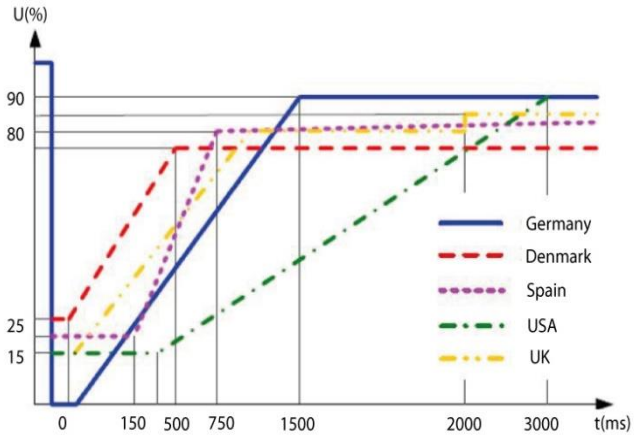


**Fig. 1.** Requirements of the WTGs during voltage dips in different countries [4].

Some researchers have proposed several active methods for LVRT, which are considered as cheaper LVRT strategies for the DFIG comparing by passive methods. To limit the rotor overcurrents, the rotor flux linkage (RFL) is controlled to follow the reduced fraction of the stator flux linkage (SFL) during the fault is proposed [16]. Also, a demagnetization control strategy is proposed to track the stator current in the opposite direction to enhance the LVRT capability of the DFIG [17, 18].

This paper presents a new LVRT strategy to maintain the DFIG based WT connected to the grid and to improve the quality of the energy supplied to the grid during voltage dips. The proposed strategy combines the active method to improve the vector control strategy in order to limit fault in current at low voltage dips and the passive method used for severe voltage dips by adding hardware protections like SDBR and DC-Chopper.

This paper is structured as: In the second section, the principle of the DFIG without the LVRT strategy is presented. In the third section, the behavior of DFIG during symmetrical grid voltage dips is analyzed. In the fourth section, the proposed LVRT control strategy is presented. The Fifth section presents the simulation results of the proposed strategy compared with the classic control strategy. Finally, the conclusions are summarized in the sixth section.

## 2. Wind system without LVRT

Fig.2 shows the system without LVRT details. The WT is connected to the DFIG rotor through a gearbox that adapts the wind speed generated from wind blades to the DFIG [19]. The grid is connected directly to the DFIG stator and to the DFIG rotor via the back-to-back converter [20, 21]. In addition, a filter is added to the grid input to attenuate harmonic effects generated by these converters.

The RSC is used in order to control the active power exchanged between the DFIG and the grid, and DFIG torque [22]. However, the GSC is used to exchange the reactive power with the grid.

The role of the Maximum Power Point Tracking (MPPT) algorithm is to optimize the energy conversion of the WT and then calculate torque reference [23]. It is used with reactive power reference and dq-axis rotor currents as inputs to the RSC control block. Thus, two Proportional-Integral (PI) controllers generate dq-axis rotor voltages. Therefore, PWM signals are generated from the RSC control block output after been transformed to abc-axis [24].

The GSC control block aims to regulate the DC-link voltage and to control the power factor [25]. Thus, the block inputs are the DC-link measured, dq-axis filtered grid currents, DC-link voltage reference, and active power reference. Therefore, PWM signals are generated from the GSC control block outputs after been transformed to abc-axis [26, 27].

## 3. DFIG modelling during symmetrical grid voltage dips.

When a fault happens in the grid, over-current and over-voltage may happen in the rotor circuit of DFIG. The level of this over-flow depends on the fault severity and location that fault had happened. The mathematical formulation regarding the occurrence of over-current in the rotor had been detailed in the reference [28, 29].

The equations of stator and rotor voltage are expressed in a reference related to the stator and rotor respectively as:

$$\overrightarrow{v_s^s} = R_s \overrightarrow{i_s^s} + \frac{d\phi_s^s}{dt} \quad (1)$$

$$\overrightarrow{v_r^r} = R_r \overrightarrow{i_r^r} + \frac{d\phi_r^r}{dt} \quad (2)$$

Where $v_s^s$ and $v_r^r$ are the stator and rotor voltages, $i_s^s$ and $i_r^r$ are the stator and rotor currents, Rs and Rr are the stator and rotor resistances, and $\phi_s^s$ and $\phi_r^r$ are the stator and rotor flux linkages. The subscripts s and r are the stator and the rotor quantities, so the superscripts s and r indicate the stator and rotor reference frames. For simplicity, the rotor variables are referred to the stator as reference frame [30, 31]. The stator and rotor flux linkages are expressed as:

$$\phi_s = L_s i_s + M i_r \quad (3)$$

$$\phi_r = L_r i_r + M i_s \quad (4)$$

Where Lr, Ls and M are respectively the rotor inductance, stator inductance and mutual inductance. With equation (3) and equation (4), the rotor flux is expressed as:

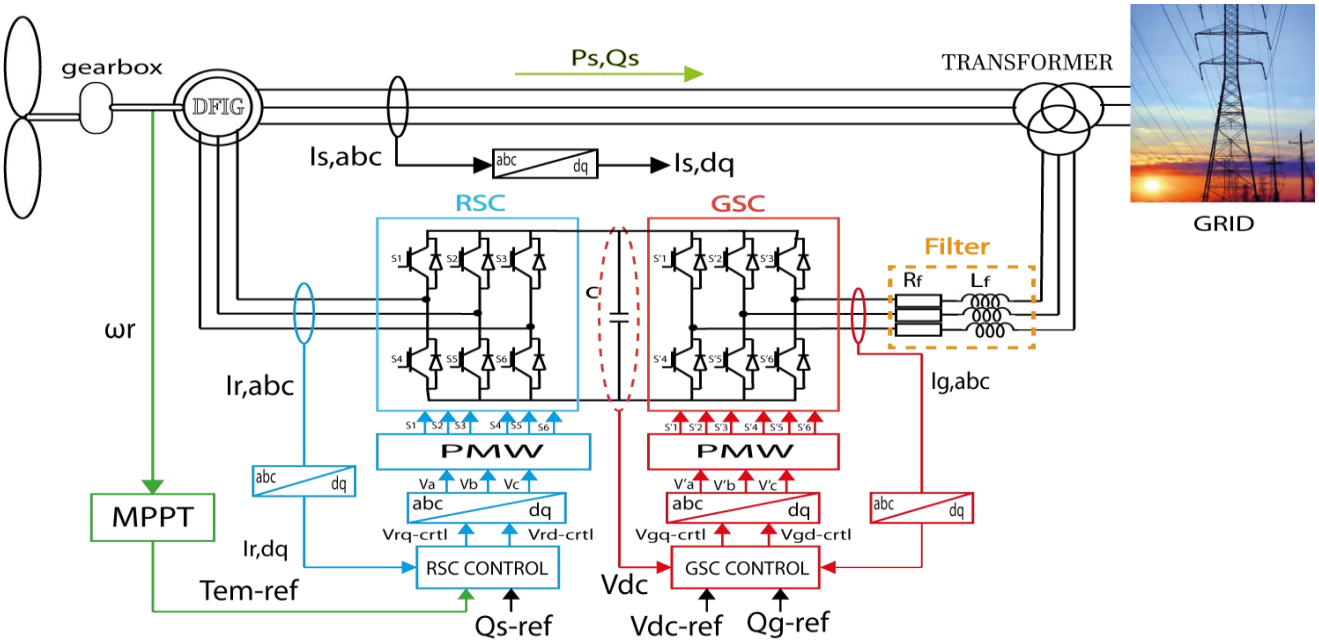


**Fig. 2.** The system without LVRT details.

$$\phi_r = \frac{M}{L_s}\phi_s + \sigma L_r i_r \quad (5)$$

Where $\sigma = 1 - {M^2}/{L_s L_r}$ is the linkage coefficient. By substituting the equation (5) into the equation (2), the rotor voltage can be expressed as:

$$\overrightarrow{v_r^r} = \overrightarrow{e_r^r} + (R_r + \sigma L_r \frac{d}{dt})\overrightarrow{i_r^r} \quad (6)$$

With:
$$\overrightarrow{e_r^r} = \frac{M}{L_s}\frac{d\phi_s^r}{dt} \quad (7)$$

From equation (6), the rotor voltage is expressed by two parts. The first one is the electromotive force defined by $e_r^r$, and then the second one which is the voltage caused by the rotor current in both the rotor circuit [26, 32].

When a symmetrical fault happens at $t = t_0$, the stator voltage decrease from $V_1$ à $V_2$:

$$\overrightarrow{v_s} = \begin{cases} V_1 e^{j\omega_s t} & t < t_0 \\ V_2 e^{j\omega_s t} & t > t_0 \end{cases} \quad (8)$$

$V_1$ and $V_2$ are respectively the stator voltage before and after grid voltage dips, and ω_s is the synchronous speed.

Neglecting Rs, the variation of the SFL during grid faults can be obtained from (1) and (8)

$$\overrightarrow{\phi_s} = \begin{cases} \frac{V_1}{jw_s} e^{j\omega_s t} & t < t_0 \\ \frac{V_2}{jw_s} e^{j\omega_s t} & t > t_0 \end{cases} \quad (9)$$

The flux is a state variable, so, it cannot undergo discontinuities. Thus, the flux cannot change instantaneously from the first value to the second one as calculated in equation (9). Instead, the flux changes progressively. As a first step, the situation in which the rotor is in an open circuit condition is analyzed [33, 34]. Using equations (1) and (3), the stator voltage becomes:

$$\overrightarrow{v_s^s} = \frac{R_s}{L_s}\overrightarrow{\phi_s} + \frac{d\overrightarrow{\phi_s}}{dt} \quad (10)$$

The expression of stator flux is calculated by solving the previous differential equation:

$$\overrightarrow{\phi_s} = \frac{V_2}{jw_s} e^{j\omega_s t} + \frac{V_1 - V_2}{jw_s} e^{-t/\tau_s} \quad (11)$$

Where $\tau_s = \frac{L_s}{R_s}$ is the time constant. The first part of the equation is the positive component of the SFL, and the second part is the DC component, which decreases with the time constant. Then according to equation (7), the electromotive force under symmetrical faults is:

$$\overrightarrow{e_r^r} = \frac{M}{L_s} V_2 s e^{jw_{sr}t} - \frac{M}{L_s}(V_1 - V_2)(1-s)e^{-t/\tau_s} e^{-j\omega_r t} \quad (12)$$

Where s is the slip, $w_{sr}$ is the difference between the synchronous speed and the rotor speed.

From equation (12) we can observe straightforwardly, that the initial value of the electromotive force induced by the DC component is large. Under 100% of voltage dip with s=-0.2, the initial amplitude of the electromotive force is

much greater than the amplitude under normal condition [35]. This is harmful to the DFIG converters.

## 4. Proposed LVRT Strategy

The proposed LVRT strategy has to manage small and severe voltage dips. In fact, the combination of the active and passive methods is proposed in this paper.

### 4.1. *Active method:*

The active method based on the control of flux, it's applied by RSC to reduce the rotor overcurrent during voltage dips. According to equations (3) and (4), the expression of rotor current is expressed as:

$$i_r = \frac{1}{L_s L_r - M^2}\left(-M\phi_s + L_s\phi_r\right) \quad (13)$$

Note that $M/L_S \approx 1$ implying:

$$i_r \simeq \frac{M}{L_s L_r - M^2}(\phi_r - \phi_s) \quad (14)$$

The equation (14) shows that the rotor current depending on the difference between rotor and stator flux linkage. When grid faults happen, the DC component and negative component will be appearing in the SFL. In this case, without a control, the RFL cannot follow the SFL properly and the difference between $\phi_s$ and $\phi_r$becomes very large, which will cause an over-current in rotor windings. Therefore, in order to reduce it during voltage dips, the RFL should be controlled to follow the SFL. Fig.3 (a) and Fig.3.(b) show the difference between the stator and rotor fluxes for 30% of voltage dip at t = 0.6s with and without control of RFL.

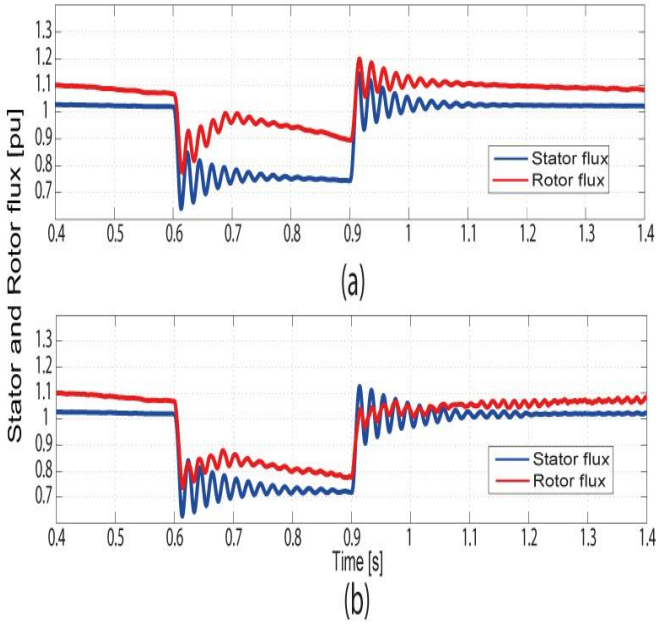


**Fig. 3.** The difference between the stator and rotor fluxes for 30% of voltage dip at t=0.6s (a) without control and (b) with control of RFL.

Fig.4 shows the control block diagram. Which is constituted of three parts. dq-axis RFL and dq-axis SFL are estimated depending on rotor and stator currents in the first block called the flux linkage detection. Then, dq-axis rotor reference is calculated depending on dq-axis stator estimated in the second block. Finally, in the RFL control block, dq-axis rotor voltages and feed-forward rotor voltages are founded.

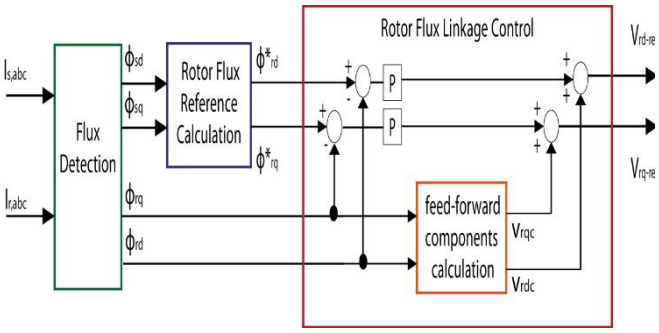


**Fig. 4.** The control block diagram.

#### *4.1.1 Flux linkage detection block:*

The role of flux linkage detection block is to determine the stator and RFL depending on the measured stator and rotor currents. In the synchronous dq-axis, the expressions of stator and rotor flux linkage are given by the equation (15).

$$\begin{cases} \Phi_{sd} = L_s I_{sd} + M I_{rd} \\ \Phi_{sq} = L_s I_{sq} + M I_{rq} \\ \Phi_{rd} = L_r I_{rd} + M I_{sd} \\ \Phi_{rq} = L_r I_{rq} + M I_{sq} \end{cases} \quad (15)$$

#### *4.1.2 Rotor flux reference calculation block*

The role of the RFL reference block is to determine the dq-axis RFL references. The RFL references are based on the SFL. Then the RFL reference $\Phi_r^*$ can be calculated by equation (16).

$$\Phi_r^* = k_T \Phi_S \quad (16)$$

Where $0 < k_T < 1$ is the tracking gain. During symmetrical faults, the SFL contains DC and negative terms as shown in the equation (11). Then, by substituting equation (16) into equation (14), the rotor current can be expressed by the equation (17).

$$i_r \simeq \frac{L_S(k_T - 1)}{L_S L_R - M^2}\Phi_s \quad (17)$$

From equations (16) and (17), the rotor current can be controlled to be smaller with a larger $k_T$ . We can calculate the minimum value of $k_T$ as follows; when a grid fault happens, the SFL increased. In other words, the initial value of the stator flux is largest during the voltage dips, and its

amplitude can be given approximately by $\phi_s(0)=\frac{V_s}{w_s}$ according to equation (9). the rotor current during the grid voltage dip will not pass the maximum current allowed. So $k_T$ should satisfy the condition expressed by equation (18):

$$\left|\frac{L_S(k_T-1)}{L_S L_R-M^2}\phi_s(0)\right| \le \left|I_{r_{max}}\right| \quad (18)$$

Where $I_{r_{max}}$ is the maximum of the rotor current. Then the expression of the minimal value of $k_T$ can be expressed as:

$$k_{T\_min} \simeq 1 - I_{r\_max}\omega_S(L_{lS}+L_{lR})/V_S \quad (19)$$

*4.1.3. Rotor flux linkage control block:*

The proportional (P) controller generates the signal from the differences between dq−axis RFL references (the RFL reference calculation block output) and dq −axis RFL (the flux linkage detection block output). Then, The dq−axis rotor voltages references are obtained by adding the control loop output to dq − axis rotor feed-forward voltages (Equations (20) and (21)). In the feed-forward components calculation, dq−axis rotor voltages are calculated according to dq−axis RFL (Equations (22) and (23)).

The interest of using the P controller instead of PI controller is to keep the RFL close to the stator flux instead of maintaining it accurately.

$$V_{rd-ref} = k_p(\phi^*_{rd} - \phi_{rd}) + V_{rdc} \quad (20)$$

$$V_{rq-ref} = k_p(\phi^*_{rq} - \phi_{rq}) + V_{rqc} \quad (21)$$

Where $k_p$ is the gain of the proportional controller, $V_{rdc}$ and $V_{rqc}$ are feed-forward components, defined as:

$$V_{rdc} = \frac{R_r M}{L_s L_r - L_s^2}\phi_{sd} + \omega_{sr}\phi_{rq} \quad (22)$$

$$V_{rqc} = \frac{R_r M}{L_s L_r - L_s^2}\phi_{sq} - \omega_{sr}\phi_{rd} \quad (23)$$

*4.1.4. Feasibility of the active method:*

The active method is limited against serious voltage dips. The choice of power converters used in the system can contribute to this limitation. In fact, changing power converters design can affect the cost of the system which is not desirable. Therefore, using active method for LVRT alone against voltage dips is not recommended. The problem during a fault is that the stator reactive power must remain within the limits imposed by the Moroccan GC. Thus, only 0.3pu of reactive power could be tolerated. So, a voltage dip caused by a grid fault has to be studied. It is a known fact that a voltage dip is characterized by two parameters: the amplitude and the duration. The maximum amplitude is demonstrated theoretically, while the duration of the maximum dip is obtained by simulation.

*a- The maximum amplitude of a voltage dip:*

To find the maximum amplitude of the voltage dip that the DFIG can handle with the active method of LVRT, a reactive power control has to be studied. Indeed the variations in the reactive power during the appearance and disappearance of the fault must be limited. To ensure a stable operation of the system, the amount of reactive power during the fault must be below a limit value of Qs=0.3pu. The Stator flux-oriented vector control is applied to the DFIG, and then the reactive power can be expressed by equation (24).

$$Q_s = 1.5 v_s i_s \quad (24)$$

With: $$i_s = \frac{1}{L_s L_r - M^2}(L_r\phi_s - M\phi_r) \quad (25)$$

Note that $M/L_r \approx 1$ and according to equations (3) and (4) $i_s$ can be approximately expressed by equation (26)

$$i_s \approx \frac{L_r}{L_s L_r - M^2}(1-k_T)\phi_s \quad (26)$$

Substituting equation (26) and equation (24), the reactive power becomes:

$$Q_s = 1.5\frac{L_r}{L_s L_r - M^2}(1-k_T)\phi_s v_s \quad (27)$$

Substituting (11) in (27), the term reactive power becomes:

$$\overrightarrow{Q_s} = 1.5\frac{L_r}{L_s L_r - M^2}(1-k_T)\left(\frac{pV_s}{jw_s}e^{j\omega_s t} + \frac{(1-p)V_s}{jw_s}e^{-\frac{t}{\tau_s}}\right)pV_s \quad (28)$$

With: V1 = Vs and V2 = pVs, where p is the level of voltage dips.

Assuming that the voltage dip occurs at t = 0s and $k_T = 0.9$, equation (28) becomes:

$$\overrightarrow{Q_s}(t=0) = 1.5\frac{L_r}{L_s L_r - M^2}(1-k_T)\frac{pV_s^2}{jw_s} \quad (29)$$

$$Q_s(t=0) < 0.3 \Rightarrow p > 0.68 \approx 0.7 \quad (30)$$

So the active method remains valid for voltage dips less than 0.3 = 30%.

*b- Maximum duration of a voltage dip*

Fig.5 shows a maximum length of the voltage dips simulation results for a voltage dip of 30%, 25%, and 23%.

In Fif.5 (a), DFIG has been subjected to a 30% of voltage dip and to several voltage dips durations. This study aims to find a dip duration that the DFIG reactive power does not exceed the tolerated value of 0.3pu required from GCs. For example, for a 30% of voltage dip and for dip duration equal to 0.4s, the reactive power exceeds 0.3pu and the value measured is 0.4pu. However, a 30% of voltage dip and for dip duration equal to 0.3s, the reactive power keeps an allowed value.

In Fig.5 (b) and Fig.5 (c), the voltage dip is decreased to 25% and to 23%. The aim of this study is to see its effects on the reactive power value. Then, for 25% of the voltage dip, the maximum duration is founded equal to 1s, and for voltage dips < 23%, it is shown that the maximum duration can exceed 1.5s. Thus, it is noticed that the maximum duration for a voltage dip changes depending on the nature of the grid fault. Therefore, for small voltage dips, the maximum dip duration of the grid fault is larger compared with deep voltage dips.

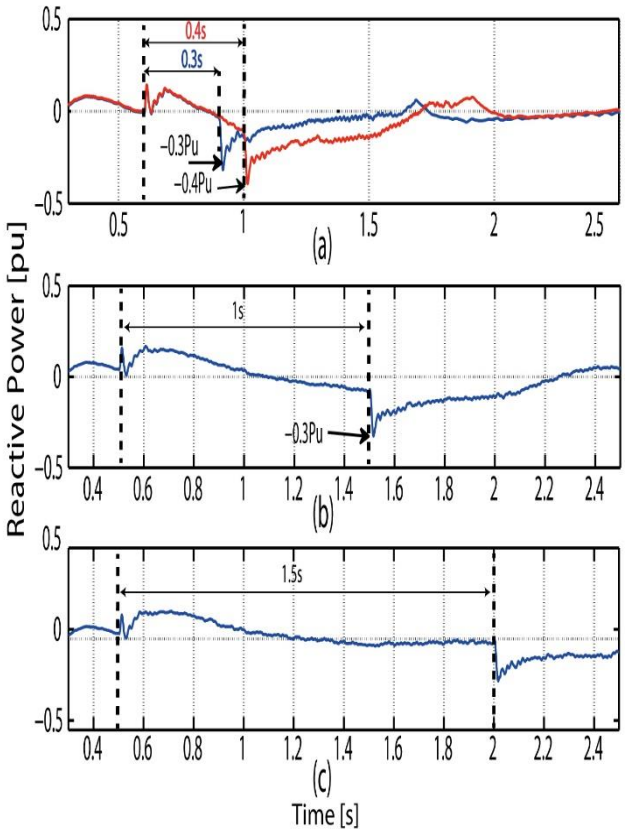


**FIG. 5.** The reactive power for voltage dips a) 30% of voltage dips, b) 25% and c) 23%.

*4.2. Passive method*

Fig.6 shows DFIG with SDBR and DC-Chopper. SDBR is connected with DFIG stator. DC-Chopper is connected between GSC and DC-link.

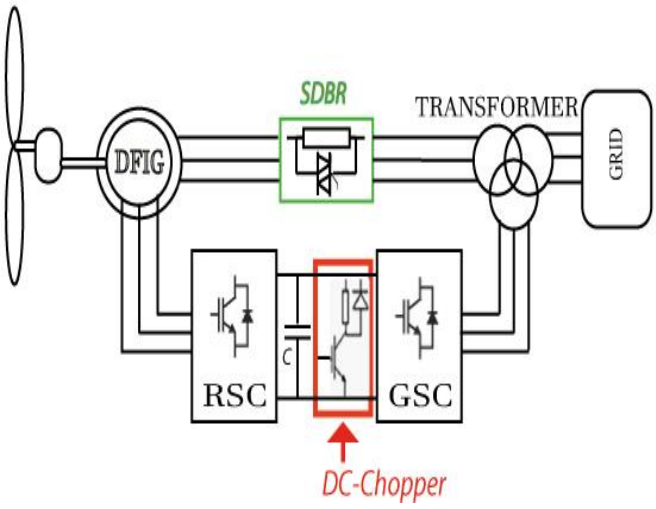


**FIG. 6.** DFIG with SDBR and DC-Chopper.

*4.2.1 Series dynamic braking resistor:*

SDBR approach is a resistor bank connected in series with stator windings. This approach has several advantages during grid faults like increasing the stator voltage and reduces the stator and rotor currents, mitigate the electrical torque and active power fluctuations. By adding SDBR to the system, an SDBR design study and its impact on the system behavior during a grid fault is required. The extreme values of the SDBR can be defined by two conditions.

The first extreme value of the SDBR is used to avoid the loss of RSC control. Thus, the minimum value of resistance that must be able to protect the RSC against rotor over-voltage during a full voltage dip has to be calculated. Equation (31) expresses the case where the value of rotor voltage during 100% of voltage dip have to not exceed the maximum RSC converter voltage.

$$e^{r}_{r,max} \leq V_{RSC,max} \qquad (31)$$

The second extreme value of the SDBR is used for stator windings protection against over-voltage during the grid faults. Therefore, this protection is provided by the maximum value of resistance. This resistance value must be able to not exceed the maximum stator voltage during grid faults. Equation (32) indicates the condition which the SDBR maximum voltage value adding to the grid voltage has to not exceed the maximum stator voltage.

$$V_{SDBR,max} + pV_1 \leq V_{Smax} \qquad (32)$$

The extreme values of the SDBR calculated according to the conditions mentioned previously (equations (31) and (32)) have been given by equation (33).

We found: $0.05pu \leq R_{SDBR} \leq 1.25\ pu$ (33)

4.2.2. DC-Chopper

The DC-Chopper is a protection device for the DC-link; his role is to short-circuits the DC-link through a power resistor during the grid voltage dips [36]. Fig.7 describes the algorithm for the operation of a DC-Chopper used in this paper. The DC-Chopper is activated only if the DC-link voltage exceeds the tolerated voltage. In normal system operation, the switch is open. Once a DC-Link voltage Vdc over-voltage is detected, the switch closes. In this case, the excess energy is dissipated across the resistor, limiting the voltage Vdc.

*4.3. Proposed active and passive methods combination*

Each method has advantages and drawbacks. The active method is used just for small voltage dips, and for maximum amplitude of 30% of voltage dips. In the other side, the passive method using SDBR approach, gives better results, even when the voltage drop is complete (100% of the voltage dip).

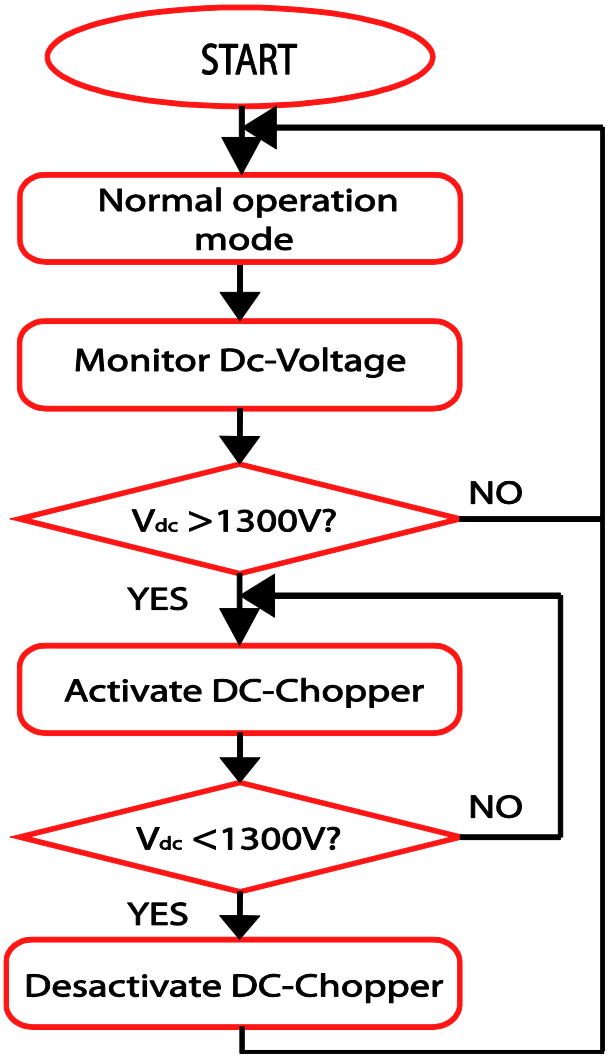


**FIG. 7.** Algorithm for the operation of a DC-Chopper.

Using the passive method for several voltage dips can damage protection components like SDBR. Thus, passive method is very expensive for every voltage dips during the grid fault.

For the reasons cited before, the new LVRT strategy is proposed to avoid inconveniences for each method (active and passive). Also, this new strategy has to manage any voltage dips types up to 100%. In addition, during voltage dips between 10% and 30%, the active method is used only and SDBR protection is disabled. In fact, in this voltage dip range, the active method is more efficient, and SDBR protection resistance is not operational and then the system cost is reduced. In the other side, for high voltage dips between 30% and 100%, only the passive method is used.

For low levels of voltage dips (between 10 - 30%), the modified control strategy is used, disabling the classic control and the hardware protection SDBR. As for large voltage dips (over 30%), the modified control strategy is disabled, and SDBR used with conventional control. Fig.8 shows the new LVRT strategy Algorithm proposed in this paper. During a normal grid operation, grid voltage and rotor current are measured in real time to check voltage dips and its nature. At the same time, a grid voltage dip is tested by measuring in real time the grid voltage and rotor current.

The first case is if the grid voltage measured is less than 0,7pu, so voltage dip is higher than 30%. Therefore, the passive method is activated only. If the dip persists, then this method is activated till the grid voltage becomes higher than 0,7pu. On the other case, if the voltage dip is less than 30%, the grid voltage measured is higher than 0,7pu. However, for a voltage dip between 10% and 30%, another condition is added which is the rotor current has to be higher than 0,85pu when the voltage dips exceed the minimum value 10%. The active method is disabled only if those two conditions are satisfied.

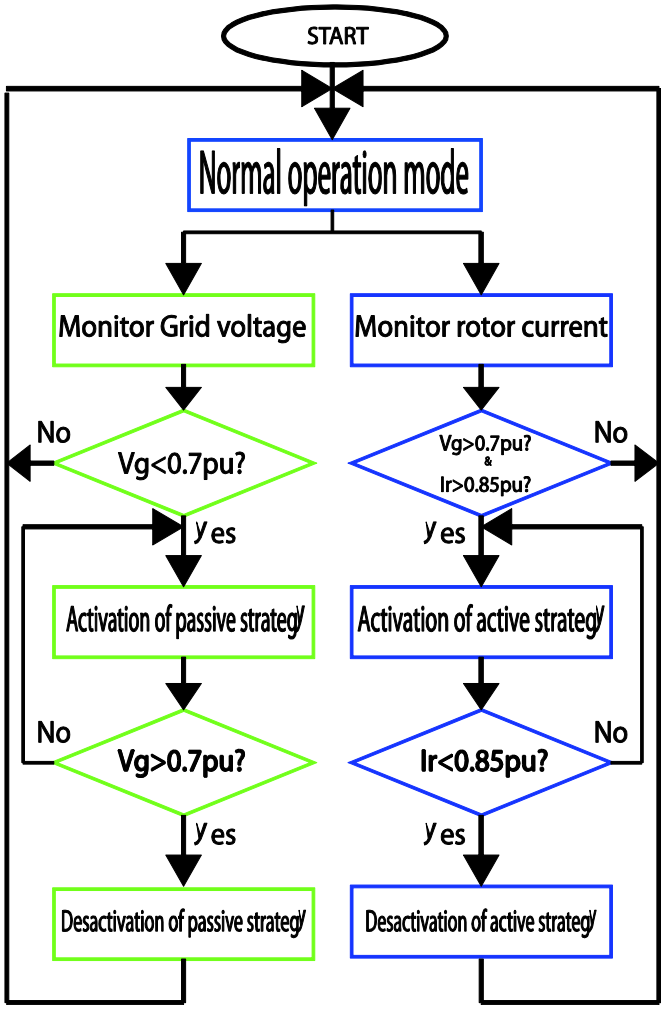


**FIG. 8.** New LVRT strategy algorithm.

## 5. Simulation results and discussion:

In this section, a new LVRT strategy applied to a DFIG will be simulated and analyzed for voltage dips during a grid fault. The MATLAB/Simulink environment and Simscape SimPowerSystems toolbox are used to model the studied system. The DFIG parameters used in this paper are given in Table 1.

To evaluate the performance of the new LVRT strategy proposed, several and successive voltage dips are used. In addition, this strategy is compared with the active method, the passive method and the system without any strategy. This study aims to demonstrate the performance of the proposed strategy. Tow voltages dips are applied to the system as shown in Fig.9.

- The first is applied at t = 0.7s, the duration is 150ms, and 100% dip.
- The second is applied at t = 1.2s, the duration is 200ms, and 25% dip.

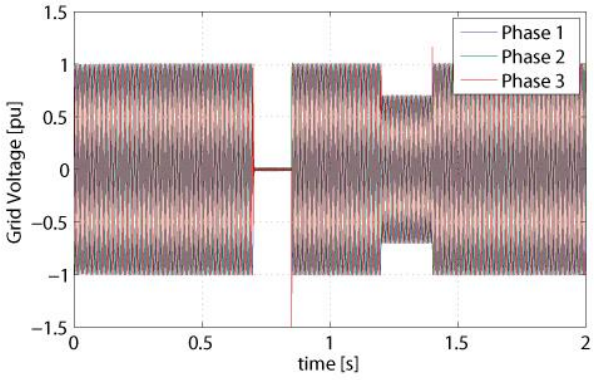


**Fig. 9.** Simulation of voltage dips applied.

**Table 1.** DFIG parameters.

| | |
|---|---|
| Stator (star connection) | |
| Rated voltage | 575 V |
| Stator resistance | 0.023 pu |
| Stator inductance | 3.08 pu |
| Mutual inductance | 2.9 pu |
| Rotor (star connection) | |
| Rated voltage | 1975 V |
| Rotor resistance | 0.016 pu |
| Rotor inductance | 3.06 pu |
| Mechanical quantities | |
| Number of pole pair P | 3 |
| Moment of inertia J | 0.685 s |
| Coefficient of friction *f* | 0.01 pu |

Fig.10 shows the simulation results of the active power. The first voltage dip of a grid fault had started at t = 0.7s, in fig.10 During the first 100% voltage dip, the active power for the Active method reaches 0.1pu which outreached the DFIG operation limit of 0,7pu and also, the DFIG is stopped. However, with the proposed method, in the active power stays in the allowed DFIG operation range (0,7pu and 1,3pu).

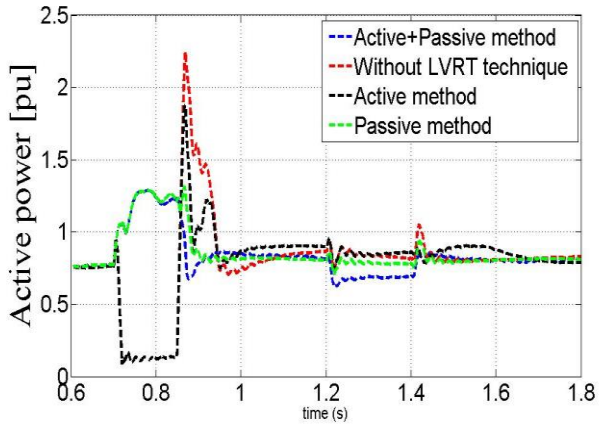


**Fig.10.** Active power [pu]

When the voltage dip is disappeared at 0,85s, the DFIG machine starts and the active power reaches 1.8pu for the active method and 2.24pu for the system without LVRT strategy. However, the proposed method respects the range of DFIG operation and doesn't detect any peak of power. The second voltage dip is 30%, then the active method is activated in this case. It is shown that the proposed strategy maintained DFIG production and the active power curve is smooth. Fig.11 shows the simulation results of the reactive power. It is shown that the proposed method respects the Moroccan grid requirement. In fact, the reactive power has to be maintained limited from 0,3pu to 0,4pu. However, the active method exceeds the reactive power allowed, which affect the grid.

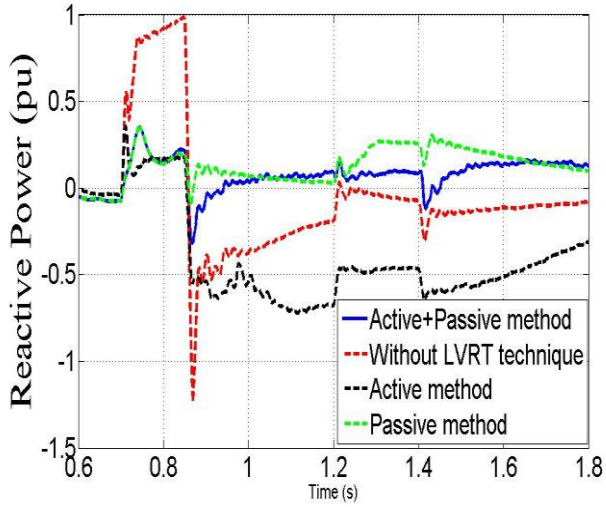


**Fig.11**. Reactive power [pu].

Fig.12 and Fig.13 show the simulation results of the rotor current and Electromagnetic torque. It is shown that the rotor current and the electromagnetic torque for the passive method and system without LVRT have serious oscillations, which is very limited near its nominal value by the proposed method. Also, for a system without LVRT, the rotor current exceeds the current permitted 2pu. In addition, it is shown that for the active method, the rotor current in the beginning of voltage dip has a dangerous peak. Those oscillations have a serious effect on the mechanical DFIG performance and on the RSC protection. In fact, a serious oscillation can damage the machine and the RSC.

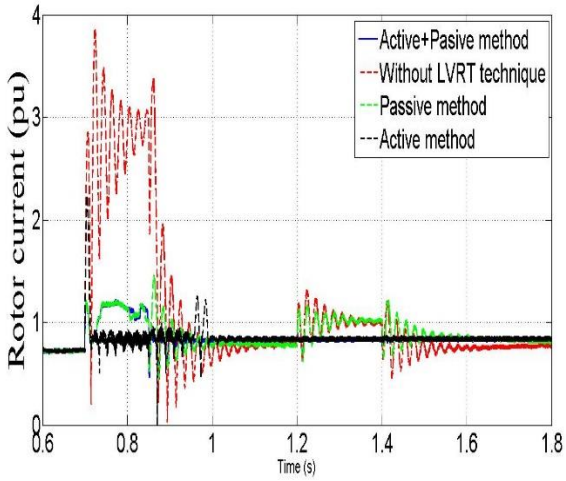


**Fig.12**. Rotor current [pu].

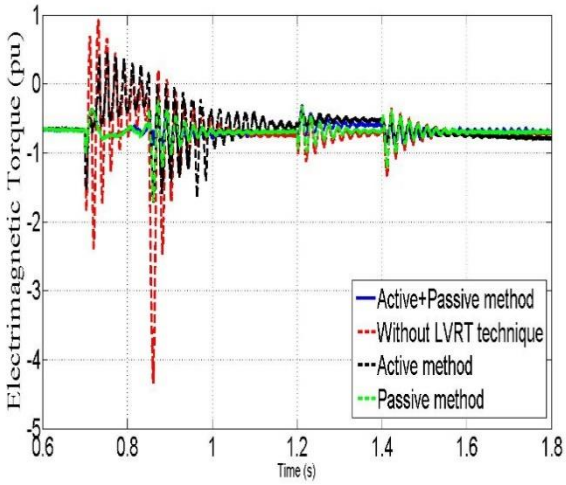


**Fig.13**. Electromagnetic torque [pu].

Fig.14 and Fig.15 show the simulation results of the stator current and the stator voltage. The stator current for the system without LVRT exceeds the maximum current permitted 2pu for the first voltage dip. Also, for the active method, passive method and system without LVRT, the stator current has serious oscillation. In addition, the stator voltage for the first voltage dip is limited for the passive and the proposed method. Also, it's limited for the second dip which active method and the proposed method.

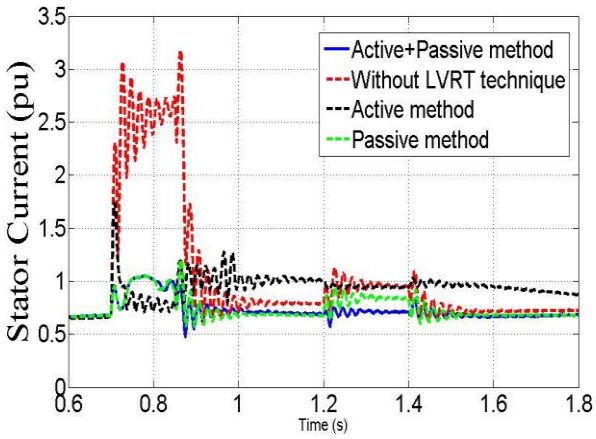


**Fig.14**. Stator current [pu].

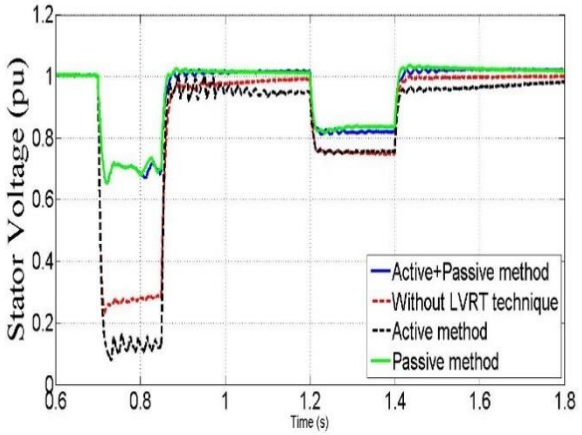


**Fig.15**. Stator voltage [pu].

Fig.16 show the simulation results of the DC-link voltage. It is shown that for the active method and without LVRT, the DC-link voltage exceeds the permitted value. The opposite of the passive method and the proposed method, which the DC-link voltage is limited to 1300V. In fact, exceeding the permitted DC-link voltage can damage the GSC protection.

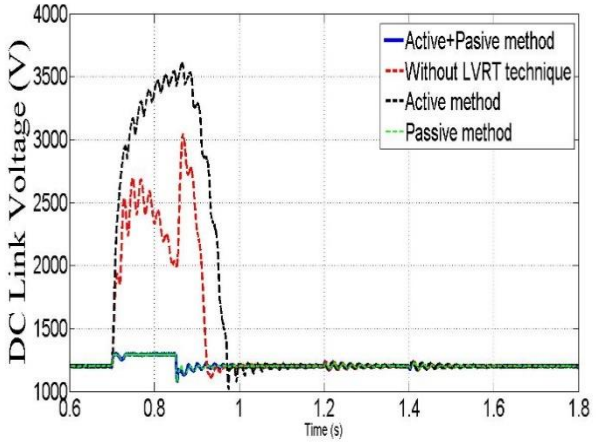


**Fig.16**. DC Link voltage [pu].

## 6. Conclusion

In this paper, we proposed a new method for LVRT strategy and compared with passive method, active method, and system without LVRT. It combines two methods. The first is the passive method, which can be used for voltage dips and especially for serious voltage dips. The second is the active method, which is based on P controller and can be used only for voltage dips less than 30%. Each method has advantages and disadvantages. In fact, the passive method is important and can be used for any voltage dip. However, using it for several voltage dips can damage it and the cost of the system can be important. In the other side, the active method is limited and can be operational only for voltage dips less than 30% but its cost is low. For these reasons, the proposed method has to exploit advantages on each method. In fact, during voltage dips between 30% and 100%, the passive method is applied. In the other hand, the proposed method becomes the active method for voltage dips between 10% and 30%. The simulation results have allowed indicating the proposed method behavior during any voltage dips. In fact, during a serious voltage dip, the passive method is used for the proposed method, also, during small voltage dips, the active method is activated. The simulation results demonstrate that the strategy proposed to protects the DFIG against over-current and keeps it connected to the grid during the voltage dip for the periods of the time imposed in the GCs.

## References

[1] Ostolaza, J. X., Etxeberria, A., & Zubia, I. (2015). Wind farm node connected DFIG/back-to-back converter coupling transient model for grid integration studies. Energy Conversion and Management, 106, 428-439.

[2] Cheng, M., & Zhu, Y. (2014). The state of the art of wind energy conversion systems and technologies: A review. Energy Conversion and Management, 88, 332-347.

[3] Mullane, A., Lightbody, G., & Yacamini, R. (2005). Wind-turbine fault ride-through enhancement. IEEE Transactions on Power Systems, 20(4), 1929-1937.

[4] Boukhris, Y., El Makrini, A., El Moussaoui, H., & El Markhi, H. (2015). Low Voltage Ride-through Capability Enhancement of Doubly Fed Induction Generator Based Wind Turbines under Voltage Dips. International Journal of Power Electronics and Drive Systems, 6(4).

[5] Wilch, M., Pappala, V. S., Singh, S. N., & Erlich, I. (2007, July). Reactive power generation by DFIG based wind farms with AC grid connection. In Power Tech, 2007 IEEE Lausanne (pp. 626-632). IEEE.

[6] Erlich, Istevan., & Bachmann, U. (2005, June). Grid code requirements concerning connection and operation of

wind turbines in Germany. In Power Engineering Society General Meeting, 2005. IEEE (pp. 1253-1257). IEEE.

[7] Lima.F.K., Luna.A., Rodriguez.P, Watanabe.E.H and Blaabjerg.F (2010). "Rotor voltage dynamics in the doubly fed induction generator during grid faults". 'IEEE Transactions on power electronics', 25(1), 118-130.

[8] Pannell, G., Atkinson, D. J., & Zahawi, B. (2010). Minimum-threshold crowbar for a fault-ride-through grid-code-compliant DFIG wind turbine. IEEE Transactions on Energy Conversion, 25(3), 750-759.

[9] Pannell, G., Zahawi, B., Atkinson, D. J., & Missailidis, P. (2013). Evaluation of the performance of a DC-link brake chopper as a DFIG low-voltage fault-ride-through device. IEEE Transactions on Energy Conversion, 28(3), 535-542.

[10] El Moursi, M. S., & Zeineldin, H. H. (2015). A parallel capacitor control strategy for enhanced FRT capability of DFIG. IEEE Transactions on Sustainable Energy, 6(2), 303-312.

[11] Okedu, K. E., Muyeen, S. M., Takahashi, R., & Tamura, J. (2012). Wind farms fault ride through using DFIG with new protection scheme. IEEE Transactions on Sustainable Energy, 3(2), 242-254.

[12] Guo, W., Xiao, L., Dai, S., Xu, X., Li, Y., & Wang, Y. (2015). Evaluation of the performance of BTFCLs for enhancing LVRT capability of DFIG. IEEE Transactions on Power Electronics, 30(7), 3623-3637.

[13] Zhang, S., Tseng, K. J., Choi, S. S., & Nguyen, T. D. (2012). Advanced control of series voltage compensation to enhance wind turbine ride through. IEEE Transactions on Power Electronics, 27(2), 763-772.

[14] Ibrahim, A. O., Nguyen, T. H., Lee, D. C., & Kim, S. C. (2011). A fault ride-through technique of DFIG wind turbine systems using dynamic voltage restorers. IEEE transactions on energy conversion, 26(3), 871-882.

[15] El Hawatt, E., et al. "Low voltage ride-through capability enhancement of a DFIG wind turbine using a dynamic voltage restorer with adaptive fuzzy PI controller." Renewable Energy Research and Applications (ICRERA), 2013 International Conference.

[16] Xiao, S., Yang, G., Zhou, H., & Geng, H. (2013). An LVRT control strategy based on flux linkage tracking for DFIG-based WECS. IEEE Transactions on Industrial Electronics, 60(7), 2820-2832.

[17] Zhou, L., Liu, J., & Zhou, S. (2015). Improved demagnetization control of a doubly-fed induction generator under balanced grid fault. IEEE Transactions on Power Electronics, 30(12), 6695-6705.

[18] Huang, Q., Zou, X., Zhu, D., & Kang, Y. (2016). Scaled current tracking control for doubly fed induction generator to ride-through serious grid faults. IEEE Transactions on Power Electronics, 31(3), 2150-2165.

[19] Abdelhafidh, M., Mahmoudi, M. O., Nezli, L., and Bouchhida, O. (2012). Modeling and control of a wind power conversion system based on the double-fed asynchronous generator. International Journal of Renewable Energy Research (IJRER), 2(2), 300-306.

[20] Medjber, Ahmed. "Comparative Study between Direct and Indirect Vector Control Applied to a Wind Turbine Equipped With a Double-Fed Asynchronous Machine Article." International Journal of Renewable Energy Research (IJRER) 3.1 (2013): 88-93.

[21] Dinesh, S., Meenakshi, R., Suhanya, M. S., Kumaran, M. S., & Muthu, R. (2014, March). Modeling and direct power control of DFIG for wind energy conversion system with a back to back converter. In Green Computing Communication and Electrical Engineering (ICGCCEE), 2014 International Conference on (pp. 1-6). IEEE.

[22] Salles, M. B. C., and A. P. Grilo. "A study on the rotor side control of DFIG-based wind turbine during voltage sags without crowbar system." Renewable Energy Research and Applications (ICRERA), 2012 International Conference.

[23] Ekanayake, J. B., Holdsworth, L., Wu, X., & Jenkins, N. (2003). Dynamic modeling of doubly fed induction generator wind turbines. IEEE transactions on power systems, 18(2), 803-809.

[24] Sarma, Nur, Judith M. Apsley, and Sinisa Djurovic. "Implementation of a conventional DFIG stator flux oriented control scheme using industrial converters." Renewable Energy Research and Applications (ICRERA), 2016 International Conference.

[25] Ferrari, Maximiliano. "GSC control strategy for harmonic voltage elimination of grid-connected DFIG wind turbine." Renewable Energy Research and Application (ICRERA), 2014 International Conference.

[26] Kumar, S., & Rawte, S. M. Grid voltage control by using DFIG during grid faults. 'IOSR Journal of Engineering (IOSRJEN)', e-ISSN: 2250-3021, p-ISSN: 2278-8719, Vol. 3, Issue 1 (Jan. 2013), ||V1|| PP 25-32.

[27] Aydin, E., A. Polat, and L. T. Ergene. "Vector control of DFIG in wind power applications." Renewable Energy Research and Applications (ICRERA), 2016 International Conference.

[28] Mendes, V. F., de Sousa, C. V., Silva, S. R., Rabelo, B., Krauss, S., & Hofmann, W. (2010, July). Behavior of doubly-fed induction generator during symmetrical voltage dips—Experimental results. In Industrial Electronics (ISIE), 2010 IEEE International Symposium on (pp. 2345-2350). IEEE.

[29] Giaourakis, Dimitrios G., Athanasios N. Safacas, and Savvas N. Tsotoulidis. "Dynamic behaviour of a wind energy conversion system including doubly-fed induction generator in fault conditions." International Journal of Renewable Energy Research (IJRER) 2.2 (2012): 227-235.

[30] Metatla, S., Mekhtoub, S., Ibtiouen, R., & Nesba, A. (2014, November). Dynamic behavior of doubly fed induction generator during network voltage dips. In Electrical Sciences and Technologies in Maghreb (CISTEM), 2014 International Conference on (pp. 1-6). IEEE.

[31] Masaud, T. M., & Sen, P. K. (2011, August). Modeling and control of doubly fed induction generator for wind power. In North American Power Symposium (NAPS), 2011 (pp. 1-8). IEEE.

[32] Lopez, J., Gubia, E., Sanchis, P., Roboam, X., & Marroyo, L. (2008). Wind turbines based on doubly fed induction generator under asymmetrical voltage dips. IEEE Transactions on Energy Conversion, 23(1), 321-330.

[33] Lopez, J., Sanchis, P., Roboam, X., & Marroyo, L. (2007). Dynamic behavior of the doubly fed induction generator during three-phase voltage dips. IEEE Transactions on Energy conversion, 22(3), 709-717.

[34] Soliman, H., Wang, H., Zhou, D., Blaabjerg, F., & Marie, M. I. (2014, September). Sizing of the series dynamic breaking resistor in a doubly fed induction generator wind turbine. In Energy Conversion Congress and Exposition (ECCE), 2014 IEEE (pp. 1842-1846). IEEE.

[35] Pannell, G., Zahawi, B., Atkinson, D. J., & Missailidis, P. (2013). Evaluation of the performance of a DC-link brake chopper as a DFIG low-voltage fault-ride-through device. IEEE Transactions on Energy Conversion, 28(3), 535-542.